

# Empirical Investigation of Properties of Lane-free Automated Vehicle Traffic\*

Milad Malekzadeh, Diamantis Manolis, Ioannis Papamichail, Markos Papageorgiou, *Life Fellow, IEEE*

**Abstract**— A new traffic paradigm has been recently proposed for automated vehicles, characterized by two combined principles: lane-free roads and vehicle nudging; the latter implying that vehicles may be influenced (nudged) by other vehicles around and even behind them. This paper presents and employs an ad-hoc vehicle movement strategy for Connected and Automated Vehicles (CAVs) driving in a lane-free environment, to investigate empirically (via simulation) some properties of the new traffic paradigm, such as the emerging fundamental diagram, traffic flow capacity, the impact of vehicle nudging, the impact of road width and more. The vehicle movement strategy is inspired by an adaptive cruise control scheme, albeit with significant modifications to account for lane-free driving, nudging, and respect of road boundaries. The movement strategy relies on real-time information to decide on longitudinal and lateral accelerations. Specifically, an "aura" is defined around each vehicle that depends on the vehicle dimensions, position, and relative speeds with surrounding vehicles. Virtual forces from surrounding vehicles are activated if these vehicles intersect with the corresponding aura. The proposed vehicle movement strategy is employed for traffic simulation on a ring-road, using a recently developed microscopic simulator called TrafficFluid-Sim, which builds on the SUMO simulation infrastructure. The achieved results demonstrate: safe (crash-free) driving at all densities; high traffic flows and capacity; increase of traffic flows and capacity via vehicle nudging; as well as via small road widening.

## I. INTRODUCTION

Traffic congestion on highways and arterials is a serious problem for big cities worldwide, resulting in significant delays, increased fuel consumption, unnecessary environmental pollution and reduced traffic safety. Traffic management measures, exploiting conventional actuators [1], [2], may delay or even circumvent the onset of congestion, if properly applied. However, increasingly emerging and future ground-breaking vehicle automation and communication technologies should also be leveraged to develop advanced solutions that can be applied within a smart road infrastructure.

Vehicle automation systems range from different kinds of driver support systems to highly or fully automated driving (i.e. SAE levels 4 and 5 vehicles); while vehicle communication enables vehicle-to-vehicle (V2V) and vehicle-to-infra-

structure (V2I) communication that may support various potential applications. During the last decade, there has been a massive effort by vehicle manufacturers and some information-technology companies, as well as research institutions to develop and deploy a variety of vehicle automation and communication systems that are transforming the vehicle capabilities [3].

Recently, the TrafficFluid concept was introduced [4], which is a novel paradigm for vehicular traffic, applicable at high levels of vehicle automation and communication systems. The TrafficFluid concept suggests lane-free traffic, whereby vehicles are not bound to fixed traffic lanes, as in conventional traffic; and vehicle nudging, whereby vehicles may exert a "nudging" effect on, i.e. influence the movement of, adjacent vehicles around and in particular also in front of them. Vehicles in a lane-free environment do not necessarily align to form lanes, but are self-organizing into dynamically changing 2-D clusters, depending on the vehicle sizes, their desired speeds, the employed vehicle movement strategies and the prevailing density, so as to maximize the available infrastructure coverage.

The low lane discipline and vehicle size diversity encountered in several developing countries motivated, in the last few years, some microscopic modelling works, which proposed models for heterogeneous and lane-less traffic; see e.g. [5], [6]. Clearly, these modelling works attempt to describe the driving behavior of real vehicles and drivers. In the case of lane-free CAV traffic, as proposed in the TrafficFluid concept, we need to design (rather than model) opportune movement strategies for safe and efficient traffic flow.

Designing a safe and efficient vehicle movement strategy in lane-free traffic is a challenging problem, and several methodological avenues may be considered to this end, including strategies based on optimal control [7], non-linear feedback control [8], as well as multi-agent systems [9]. For quick verification and demonstration of the TrafficFluid concept, an ad-hoc vehicle movement strategy for lane-free roads was developed [10] at an early stage. An improved and strongly modified ad-hoc strategy for lane-free traffic is described in Section II. Then, simulation results are presented in Section III, using a recently developed microscopic simulator, called TrafficFluid-Sim [11], which builds on the SUMO simulation infrastructure [12]. The paper concludes with Section IV.

## II. VEHICLE MOVING STRATEGY

Designing a safe and efficient vehicle movement strategy in lane-free traffic is a challenging problem, and, as men-

\* The research leading to these results has received funding from the European Research Council under the European Union's Horizon 2020 Programme / ERC Grant Agreement no. 833915, project TrafficFluid, see: <https://www.trafficfluid.tuc.gr>.

All authors are with the Dynamic Systems and Simulation Laboratory, Technical University of Crete, Chania 73100, Greece. Markos Papageorgiou is also with the Faculty of Maritime and Transportation, Ningbo University, Ningbo, China. (e-mails: [mmalek@dssl.tuc.gr](mailto:mmalek@dssl.tuc.gr); [dmanolis@dssl.tuc.gr](mailto:dmanolis@dssl.tuc.gr); [ipapa@dssl.tuc.gr](mailto:ipapa@dssl.tuc.gr); [markos@dssl.tuc.gr](mailto:markos@dssl.tuc.gr)).

tioned in the Introduction, several methodological avenues may be considered to this end. For quick verification and demonstration of the TrafficFluid concept, an ad-hoc vehicle movement strategy for lane-free roads has been developed and is described here.

In this study, the double-double-integrator (DDI) model is employed to define the vehicle's motion dynamics based on the following kinematic equations for 2-D vehicle position and speed

$$\begin{aligned} x(t+T) &= x(t) + v_x(t)T + 0.5f_x(t)T^2 \\ v_x(t+T) &= v_x(t) + f_x(t)T \\ y(t+T) &= y(t) + v_y(t)T + 0.5f_y(t)T^2 \\ v_y(t+T) &= v_y(t) + f_y(t)T \end{aligned} \quad (1)$$

for  $t = 0, T, 2T, \dots$ . Thus, at the beginning of each time-step  $t$  of length  $T$ , each vehicle departs from position  $(x(t), y(t))$ , that is actually the center of the vehicle, with longitudinal (lateral) speed  $v_x(t)$  ( $v_y(t)$ ); and, moving with constant longitudinal (lateral) acceleration  $f_x(t)$  ( $f_y(t)$ ), it reaches its updated state (positions and speeds) at time  $t+T$ . In the above equations, the acceleration value is considered as a control input to be specified by the moving strategy. The DDI model is deemed appropriate for vehicle movement that does not involve strong turnings, as it is typically the case on highways.

In the proposed control scheme, longitudinal (x-direction) and lateral (y-direction) accelerations for each vehicle at time  $t$  are computed via the following respective equations:

$$\begin{aligned} f_x(t) &= \sigma_x^{fs} f_x^{fs}(t) + f_x^{fp}(t) + \sigma^{ng} \gamma_x f_x^{ng}(t) \\ f_y(t) &= f_y^{fs}(t) + f_y^{fp}(t) + \sigma^{ng} \gamma_y f_y^{ng}(t) \end{aligned} \quad (2)$$

The purpose of each "force" on the right-hand side of (2) is briefly described as follows:

- The *target-speed forces*  $f_x^{fs}$  and  $f_y^{fs}$  strive for the vehicle to attain its respective longitudinal and lateral target speeds.  $f_x^{fs}$  is not active all the time. The activation of this term depends on the situation of the vehicle with respect to surrounding vehicles and will be described comprehensively later. Activation or deactivation of  $f_x^{fs}$  is performed using the binary variable  $\sigma_x^{fs} \in \{0,1\}$ .
- The *repulsive forces*  $f_x^{fp}$  and  $f_y^{fp}$  are present due to vehicles ahead (downstream) and aim at preventing collision with such vehicles.
- The *nudging forces*  $f_x^{ng}$  and  $f_y^{ng}$  are present due to vehicles behind (upstream) and may facilitate advancement of faster vehicles behind, but have also an impact on the macroscopic characteristics of the emerging traffic flow [13]. The coefficients  $\gamma_x, \gamma_y \in [0,1]$  adjust the effect of nudging forces versus repulsive forces; enabling attenuation of nudging forces if desired. The nudging forces  $f_x^{ng}$  and  $f_y^{ng}$  may under circumstances have to be de-activated, and this is performed using the binary variable  $\sigma^{ng} \in \{0,1\}$ .

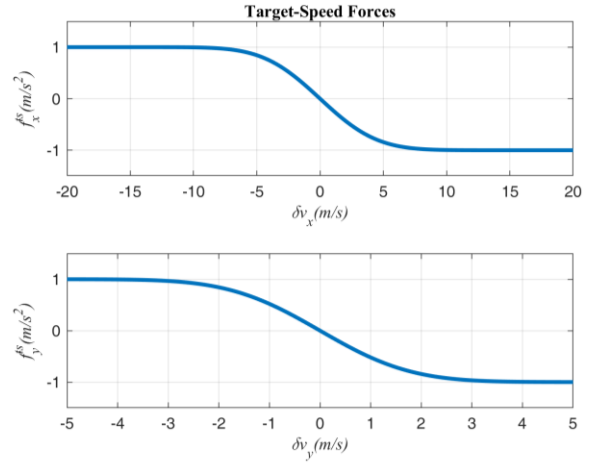


Figure 1. The target-speed forces providing deceleration or acceleration, as needed, to address deviations  $\delta v = v - v_d$  from a desired speed.

It should be noted that the nudging force is one of the novel characteristics introduced with the TrafficFluid paradigm. Vehicles communicate their presence to other vehicles (or are sensed by them), and this may exert a "nudging" effect on the vehicles in front (under circumstances and to an extent to be specified later), i.e., vehicles in front may experience (apply) a pushing force, e.g., in the direction of the line connecting the centers of the nudging vehicle and the nudged vehicle.

#### A. Target-speed Forces

Each vehicle is assigned a desired (non-zero) longitudinal speed  $v_x^d$  and a (typically equal to zero) lateral desired speed  $v_y^d$ . When a vehicle is moving below, at, or above its longitudinal (lateral) desired speed,  $f_x^{fs}$  ( $f_y^{fs}$ ) becomes positive, zero, or negative, respectively. More specifically, we have the following functions, used for their suitable sigmoid shape (illustrated in Fig. 1)

$$\begin{aligned} f_x^{fs}(t) &= \operatorname{erfc}[0.2(v_x(t) - v_x^d)] - 1 \\ f_y^{fs}(t) &= \operatorname{erfc}[0.5(v_y(t) - v_y^d)] - 1 \end{aligned} \quad (3)$$

where  $\operatorname{erfc}(x) = \frac{2}{\sqrt{\pi}} \int_x^\infty e^{-t^2} dt$ .

#### B. Repulsive Forces

A repulsive force is created for each couple of adjacent vehicles  $i$  and  $j$ , with a direction along the line connecting both vehicle centers. The repulsion force indicates towards, and applies to, the vehicle, whose center is farther upstream. We denote the vehicle widths  $w_i$  and  $w_j$ .

The following function defines the repulsive force magnitude for a vehicle  $i$  due to the presence of a downstream vehicle  $j$

$$\Pi(\Delta x, \Delta y, \Delta v_x, L_y, D_y) = F(\Delta x, \Delta v_x) \cdot H(\Delta y, L_y, D_y) \quad (4)$$

where  $F(\Delta x, \Delta v_x)$  is a function depending on longitudinal arguments, notably the longitudinal distance  $\Delta x = x_j - x_i$  and the longitudinal relative speed  $\Delta v_x = v_{jx} - v_{ix}$  for vehicles  $i$

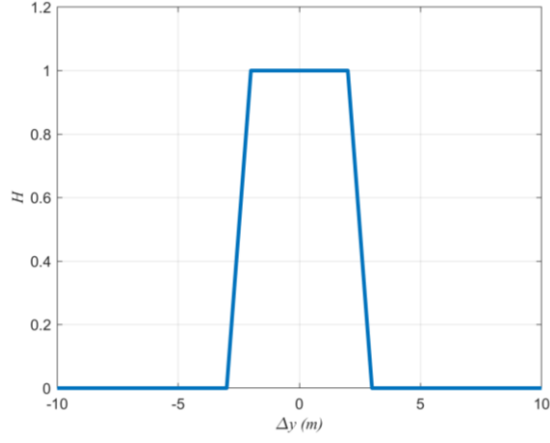


Figure 2. The function  $H(\Delta y, L_y, D_y)$  versus  $\Delta y$  for  $L_y = 1, D_y = 2$ .

and  $j$ . This function is inspired from lane-based car-following ACC (Adaptive Cruise Control) laws [14], as will be described later. The function  $F(\Delta x, \Delta v_x)$  is multiplied with another function that depends on lateral arguments only, as follows

$$H(\Delta y, L_y, D_y) = \max \left\{ 0, \min \left\{ 1, 1 - \frac{\Delta y - D_y}{L_y}, \frac{\Delta y + D_y + L_y}{L_y} \right\} \right\} \quad (5)$$

For given values of the non-negative arguments  $L_y, D_y$ , the shape of this function versus the lateral distance  $\Delta y = y_j - y_i$  between vehicles  $i$  and  $j$  is a trapezoid with height equal to 1 and basis equal to 0, as displayed in Fig. 2.

Effectively, the force magnitude  $\Pi$  rises linearly from 0 to  $F(\Delta x, \Delta v_x)$  within the interval  $\Delta y \in [-L_y - D_y, -D_y]$ ; remains constant at value  $F(\Delta x, \Delta v_x)$  within  $\Delta y \in [-D_y, D_y]$ ; and drops linearly to 0 within  $\Delta y \in [D_y, D_y + L_y]$ . Thus, the function  $H(\Delta y, L_y, D_y) \in [0, 1]$  determines how much of the car-following force  $F(\Delta x, \Delta v_x)$  actually applies, depending on the lateral vehicle displacement  $\Delta y$ . This is because the car-following repulsion is mainly necessary if both vehicles are longitudinally aligned on the 2D road surface (considering also their respective widths); but it may gradually fade to zero, as the lateral displacement increases, since a collision of both vehicles becomes increasingly irrelevant. As any two vehicles may be moving laterally towards each other,  $L_y$  must also reflect accordingly the lateral relative speed between the two vehicles  $i$  and  $j$ , if relevant. More specifically,

$$L_y = \max \left\{ 0, (v_{yi} - v_{yj}) \text{sign}(y_j - y_i) T_y \right\} + L_{sy}, \quad (6)$$

where  $T_y$  is a lateral time-gap and  $L_{sy}$  is a safety distance.  $D_y$  in (5) equals the sum of half-widths of the two vehicles, plus a safety distance  $D_{sy}$ .

$$D_y = 0.5(w_i + w_j) + D_{sy}. \quad (7)$$

In summary, the upstream vehicle  $i$  receives, due to the downstream vehicle  $j$ , a repulsion force  $f_j^{rp}$ , with magnitude  $|f_j^{rp}| = \Pi \in [0, F(\Delta x, \Delta v_x)]$ .

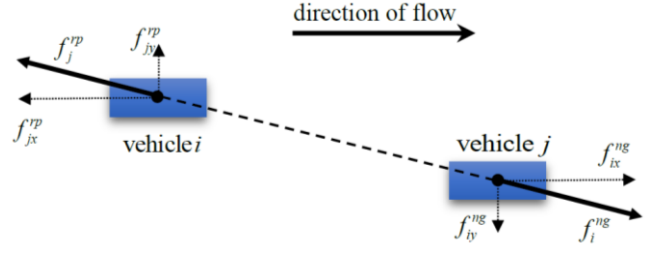


Figure 3. Visualization of repulsive and nudging forces between two vehicles.

### C. Nudging Forces

The downstream vehicle  $j$  receives, due to the upstream vehicle  $i$ , a nudging force  $f_i^{ng}$  with a magnitude  $|f_i^{ng}| = |f_j^{rp}|$ , which, however, can be moderated by the choice of the aforementioned parameters  $\gamma_x, \gamma_y$ . Figure 3 depicts how two vehicles affect each other by applying repulsive and nudging forces.

### D. The Action Graph

We turn now our attention to the description of the car-following force  $F(\Delta x, \Delta v_x)$ . Figure 4 displays an Action Graph (AG) in  $(\Delta x, \Delta v_x)$ -coordinates of the relative longitudinal speed  $\Delta v_x$  versus the longitudinal distance  $\Delta x$  between the downstream vehicle  $j$  (leader) and the upstream vehicle  $i$  (follower) [14], [15].

The AG is separated in different areas, with corresponding actions in each of them, depending on the measured  $(\Delta x, \Delta v_x)$  for the couple of vehicles. The actions refer to the follower, i.e., the vehicle whose center is further upstream. For example, if the leader has higher speed than the follower ( $\Delta v_x > 0$ ), no repulsion is necessary, and the follower could accelerate to its desired speed. If the leader has a speed lower than the follower ( $\Delta v_x < 0$ ), then the follower may have to decelerate etc. Three distinct areas have been selected: *no-repulsion area*, where the follower strives to reach its desired speed; *deceleration area*, where appropriate deceleration is activated; and *emergency area*, where full break is activated for collision avoidance. These

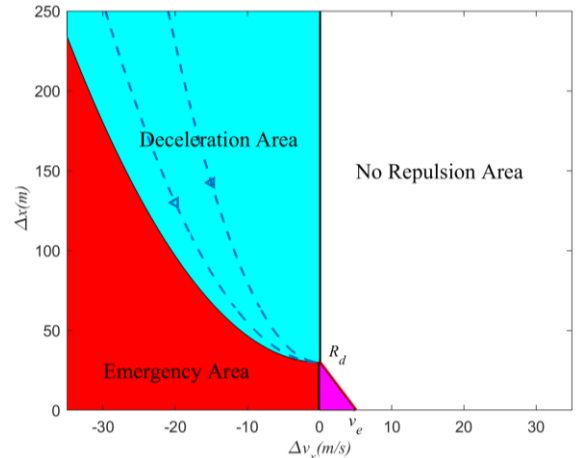


Figure 4. Action Graph for the acceleration strategy depending on longitudinal distance and relative speed between the vehicles  $j$  and  $i$ .

areas and corresponding actions are described in what follows.

*No-Repulsion area:* This includes non-critical situations, where the leader is faster than the follower, and, as a consequence, no repulsion action is necessary, i.e.  $F(\Delta x, \Delta v_x) = 0$ .

*Deceleration area:* In this area, the current leader's speed is lower than the follower's ( $\Delta v_x < 0$ ) at relatively close distance  $\Delta x$ , hence the follower should decelerate. According to the widespread constant time-gap policy in lane-based car-following for automated vehicles, we consider in AG the set-point  $(R_d, 0)$ , see Fig. 4, where  $R_d = d_s + v_j T_x$ ,  $T_x$  is a longitudinal time-gap and  $d_s$  is a safety distance. The point  $(R_d, 0)$  represents a set-point for the follower. For passenger convenience, we select to apply constant deceleration for the following vehicle, so as to reach this set-point, departing from any position  $(\Delta x, \Delta v_x)$  within the deceleration area. Such a constant deceleration may be readily computed to be [15]

$$D = \frac{1}{2} \frac{\Delta v_x^2}{\Delta x - R_d}. \quad (8)$$

Then, if the leader maintains its speed constant, the resulting path in the AG is given by the parabola  $\Delta x = R_d + \Delta v_x^2 / 2D$ , which leads directly to the set-point; see Figure 4 for some such parabolas. Of course, the leader may be changing speed, hence, executing (8) in real time, with continuously updated measurements  $(\Delta x, \Delta v_x)$ , corresponds to a model predictive control (MPC) scheme towards the set-point  $(R_d, 0)$ .

Note that the boundary between the deceleration area and the emergency area is also defined by such a parabola for a limit deceleration, e.g.  $D = 2.5 \text{ m/s}^2$ . In conclusion, if  $(\Delta x, \Delta v_x)$  lies in the deceleration area, the follower decelerates, and  $F(\Delta x, \Delta v_x)$  equals  $D$  given by equation (8).

*Emergency area:* The red and the magenta zones in Fig. 4 correspond to the emergency area that includes two regions. If relative speed is negative, and the coordinates  $(\Delta x, \Delta v_x)$  are under the emergency parabola, the vehicle is in the red zone of the emergency area. In this zone, the vehicle must decelerate as hardly as possible, and  $F(\Delta x, \Delta v_x)$  equals the limit deceleration, e.g.,  $2.5 \text{ m/s}^2$ . In case the relative speed is small positive, i.e., we are on the right-hand side of the AG close to the vertical axis, but at small distance between vehicles, a crash risk may still be imminent. Therefore, we extend the emergency area to the right-hand side of the AG to create a safe margin (magenta zone in Figure 4), with  $F(\Delta x, \Delta v_x)$  therein taken equal to half of the limit deceleration, e.g.,  $1.25 \text{ m/s}^2$ . Hence, if the relative speed is positive and the coordinates  $(\Delta x, \Delta v_x)$  are under the line  $\Delta x = R_d - R_d \Delta v_x / v_e$ , the vehicle remains in the emergency area, albeit it applies a smoother deceleration.

#### E. Accumulating Repulsive and Nudging Forces

The repulsive force  $f^{rp}$ , acting on a reference vehicle  $i$ , equals the sum of individual repulsive forces  $f_j^{rp}$ , for all  $j \in S_i^{rp}$ , where the set  $S_i^{rp}$  is defined as containing at most

$n^{rp}$  downstream vehicles; namely those with the strongest repulsive force magnitude within a longitudinal distance  $\Delta$ . Similarly, the nudging force  $f^{ng}$ , acting on a reference vehicle  $i$ , equals the sum of individual nudging forces  $f_j^{ng}$ , for all  $j \in S_i^{ng}$ , where the set  $S_i^{ng}$  is defined to contain at most  $n^{ng}$  upstream vehicles; namely those with the strongest nudging force magnitude on  $i$  within the backward distance  $\Delta$ .

The parameter  $\sigma_x^{is}$  in (2) is equal to one, only if the set  $S_i^{rp}$  is empty, i.e. only if no repulsion is applied to the reference vehicle by downstream vehicles. Also, when the strongest repulsive force of the set  $S_i^{rp}$  has a magnitude more than  $2.0 \text{ m/s}^2$ , the parameter  $\sigma^{ng}$  for vehicle  $i$  are set equal to zero, in order to avoid any nudging influence from upstream. Otherwise, this parameter is equal to one.

#### F. Acceleration Bounds and Smoothing

After  $f_x$  and  $f_y$  have been produced from the respective sums of target-speed, repulsive and nudging forces, a constraining mechanism is applied before they are used as accelerations.

To start with, longitudinal and lateral accelerations are bounded to lie within specified respective ranges  $f_x \in [u_x^{b-}, u_x^{b+}]$  and  $f_y \in [u_y^{b-}, u_y^{b+}]$ .

As a consequence of nudging forces, a vehicle might excessively exceed its desired speed. Moreover, due to repulsive forces, a vehicle might move backwards. In order to prevent both of these occurrences, the longitudinal acceleration  $f_x$  is truncated to remain within the range  $[-v_x/T, ((1+\alpha)v_d - v_x)/T]$ , effectively preventing a vehicle's longitudinal speed from exceeding  $(1+\alpha)v_d$ , with  $\alpha > 0$ , or from moving backwards.

The lateral acceleration  $f_y$  is truncated to remain within the range  $[-(\beta v_x + v_y)/T, (\beta v_x - v_y)/T]$ , so that the lateral speed will never exceed a fraction  $\beta \in (0, 1]$  of the current longitudinal speed, in either direction. This bound is introduced to ensure that the resulting vehicle paths remain feasible, despite the independent longitudinal and lateral control implied by the DDI model. Roughly speaking, the vehicle cannot move fast sideward if it is not moving sufficiently fast forward.

Lateral speed must also be bounded for safety reasons by a specific maximum and minimum limit  $v_{y\_max} = -v_{y\_min}$ , and, to this end, the lateral acceleration  $f_y$  is truncated to remain within the range  $[(v_{y\_min} - v_y)/T, (v_{y\_max} - v_y)/T]$ .

In order to keep a vehicle within the boundaries of the highway, additional lateral acceleration constraints are required. This task may be addressed as a regulation problem, whereby a (left or right) road boundary is considered as a reference lateral position, and a lateral acceleration of the vehicle is obtained via a boundary feedback controller, such that the vehicle moves asymptotically towards the boundary, or remains on the boundary, without violating it. Consequently, such an acceleration can be used as a lateral acceleration *bound* to ensure that the vehicle will never cross the corresponding road boundary.

For the design of the boundary feedback controller, consider the double-integrator dynamics for the lateral movement of a vehicle, which are part of the set of equations (1). We define the regulation errors regarding the vehicle's lateral position and lateral speed, as follows

$$\begin{aligned} e_1(t) &= y(t) - \hat{y}(t) \\ e_2(t) &= v_y(t) - \hat{v}_y(t) \end{aligned} \quad (9)$$

where  $\hat{\cdot}$  are reference values. In the case of a straight road (or unfolded ring-road, as considered in the following section for simulation purposes), the right boundary of the road corresponds to  $\hat{y}(t) = w/2$ , due to the width  $w$  of the vehicle; while the left boundary of the road corresponds to  $\hat{y}(t) = W - w/2$ , where  $W$  is the width of the road. Additionally, since the road is straight, we have the reference lateral speed  $\hat{v}_y(t) = 0$ .

We now consider the following state-feedback boundary controller for the lateral acceleration of the vehicle

$$f_y(t) = -k_1 e_1(t) - k_2 e_2(t) \quad (10)$$

where  $k_1$  and  $k_2$  are feedback gains. From (1) and (9)-(10), we get the following state equation for the regulation error for the case of a straight road:

$$\begin{bmatrix} e_1(t+T) \\ e_2(t+T) \end{bmatrix} = \begin{bmatrix} 1 - \frac{k_1 T^2}{2} & T - \frac{k_2 T^2}{2} \\ -Tk_1 & 1 - Tk_2 \end{bmatrix} \begin{bmatrix} e_1(t) \\ e_2(t) \end{bmatrix}. \quad (11)$$

The characteristic equation for (11) is

$$Z^2 + (Tk_2 - 2 + \frac{k_1 T^2}{2})Z + (1 - Tk_2 + \frac{k_1 T^2}{2}) = 0. \quad (12)$$

The boundary controller should exhibit asymptotic behavior towards the target values, as any position overshooting might lead to boundary violation. Thus, for stability and aperiodic response, we select the gains such that the characteristic equation (12) has two equal real non-negative stable roots. This leads to the following necessary conditions for the gains:

$$\begin{aligned} (Tk_2 - 2 + \frac{k_1 T^2}{2})^2 - 4(1 - Tk_2 + \frac{k_1 T^2}{2}) &= 0 \\ 0 < 2 - Tk_2 - \frac{k_1 T^2}{2} < 2 \end{aligned} \quad (13)$$

Simplifying the above relations, we get

$$\begin{aligned} k_2 &= 2\sqrt{k_1} - k_1 T / 2 \\ 0 < k_1 < 1/T^2, \quad 0 < k_2 < 3/2T \end{aligned} \quad (14)$$

The above conditions allow for a range of values for the gains. If the gains are selected too fast, then the controller (10) might lead to acceleration bounds that are not feasible, given the constant lateral acceleration bounds mentioned earlier. On the other hand, if the gains are selected too slow, then the resulting bounds may be too conservative and be

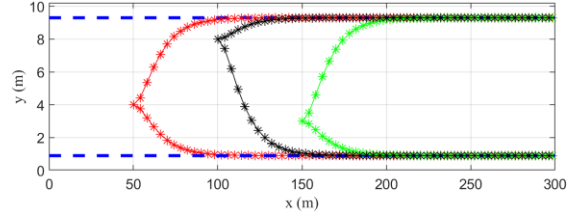


Figure 5. Trajectories for three different vehicles (red; black and green) following the upper and lower bounds of acceleration.

activated, although no boundary violation is imminent. As suitable trade-off, the controller gains may be selected so as to avoid both too strong vehicle maneuvers and premature bound activation.

In summary, using (10), with appropriate gains, we compute, at each time step, two respective accelerations for the left and right road boundaries. These accelerations are used as upper and lower bounds, respectively, of the lateral vehicle acceleration, which guarantee that no boundary violation occurs; and also enable the vehicle to be driving exactly on the boundary, if necessary.

As an illustration example for the behavior of the boundary controller, Fig. 5 presents the trajectories that three (independent) vehicles (red, black and green) would follow, starting from different initial positions  $(x, y)$ , if they would directly apply a lateral acceleration computed via (10) with gains  $k_1 = 4 \text{ s}^{-2}$  and  $k_2 = 3.75 \text{ s}^{-1}$ . More precisely, the initial vehicle positions are (50,4) for the red vehicle; (100,8) for the black vehicle; and (150,3) for the green vehicle; while the width of the road,  $W$ , is 10.2 m, and the width of the vehicles,  $w$ , is 1.8 m. For all vehicles, the initial lateral speed is equal to zero, and the longitudinal speed is constant and equal to 20 m/s. For each vehicle, we draw two trajectories, one with set-point corresponding to the left road boundary, and another with set-point corresponding to the right road boundary. It may be seen in Fig. 5, that the vehicles, driven laterally by the boundary controller (10), would asymptotically approach the respective boundary and remain there.

Of course, the boundary controller (10) is not meant to continuously drive the vehicles, but merely to present lateral acceleration bounds so as to avoid road boundary violations. Thus, a vehicle will generally follow a lateral acceleration that is not equal to an acceleration bound, unless the vehicle is close to the road boundary and is being nudged towards it by another vehicle. This situation is presented in Fig. 6, displaying lateral acceleration, lateral speed and lateral position over time (blue trajectories) for a vehicle, as extracted from one of the multi-vehicle simulations reported in the next section. The vehicle's lateral acceleration is bounded by two constant bounds (black lines) and two time-variant bounds (red lines), the latter computed via (10) for the respective left and right road boundaries. Note that the lower time-variant bound is not visible in the plot, as it is in the order of  $-30 \text{ m/s}^2$ . At the start ( $t=1000 \text{ s}$ ) of the depicted trajectories, the vehicle is close to the left road boundary, but without imminent boundary violation; hence the red time-

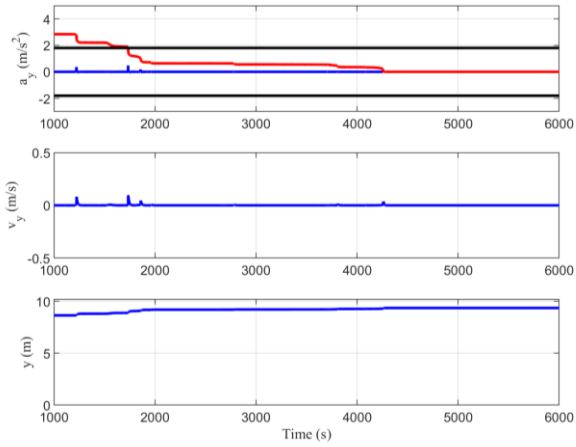


Figure 6. Trajectories over time for a vehicle that is close to the left road boundary and is nudged toward it.

varying boundary is seen to be remote. However, during time-period [1000, 4200] s, the vehicle experiences a number of light lateral nudges by other vehicles and approaches the road boundary closer. This leads to a corresponding lowering of the time-variant upper bound (red line), until, at around 4300 s, the bound is activated and takes control of the lateral vehicle movement. This leads the lateral vehicle position asymptotically to the road boundary; and maintains it there, as the lateral speed and lateral acceleration converge to zero.

Finally, the longitudinal acceleration  $f_x(t)$  produced over time (after bounding) is smoothed, before applying it to (1), using an exponential filter with a smoothing factor  $a_s$ . This is in order to mitigate possible strong and abrupt acceleration changes over time, that may present a discomfort for the passengers of the vehicles.

### III. SIMULATION RESULTS

Some simulation-based experiments were designed by use of the ad-hoc vehicle movement strategy described in Section II, in order to highlight and demonstrate some basic features of the TrafficFluid concept. The described vehicle movement strategy is employed for traffic simulation on a ring-road using a recently developed microscopic simulator called TrafficFluid-Sim [11], which builds on the SUMO simulation infrastructure [12]. Figure 7 shows a snapshot of the simulation environment.

Specifically, we produced four fundamental diagrams (FDs), i.e. flow-versus-density stationary relations, for six corresponding scenarios of vehicle movement, as follows:

- No nudging forces applied ( $\gamma_x = 0, \gamma_y = 0$ );
- Weak nudging forces applied ( $\gamma_x = 0.5, \gamma_y = 0.5$ );
- Nominal (full) nudging forces applied ( $\gamma_x = 1, \gamma_y = 1$ );
- Nominal nudging forces applied and incremental widening of the road for three different increments.

Each FD (see Fig. 8) was obtained by simulating the movement of  $n$  vehicles (for multiple  $n$  values), governed by the described movement strategy, on a (two-dimensional)

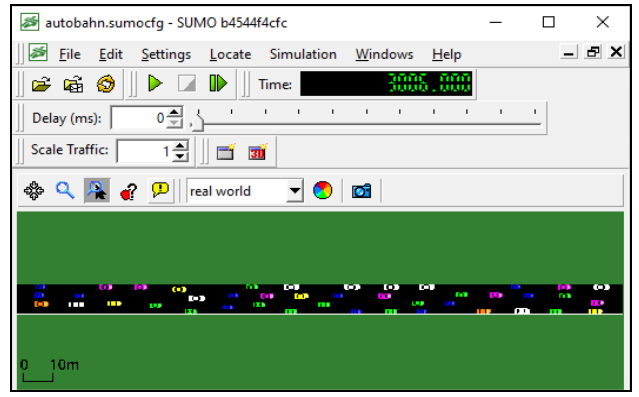


Figure 7. A snapshot of the simulation environment TrafficFluid-Sim.

ring-road, which is 1 km long and 10.2 m wide (corresponding to the width of 3 conventional lanes) for the first three scenarios; while the road was widened by 0.425 m, 0.85m and 1.7 m (one eighth, one quarter and one half of a conventional lane width) for the last three scenarios.

Let  $(x(t), y(t))$  denote the position of (the center of) a vehicle at time  $t$  during the simulation. Initially, at  $t = 0$ , each vehicle is placed at some location  $(x(0), y(0))$ , such that all  $n$  vehicles are randomly and quasi-uniformly distributed on the 2-D road surface. To this end, we start with the lateral distribution and assign the vehicles to three zones (corresponding to "lanes"), with small lateral alignment imperfections. More specifically, the  $n$  vehicles are equally divided into three (as many as lane-widths) parallel zones  $l = 1, 2, 3$ ; and each zone is centered at  $y_l = 1.7 + 1.7(l - 1)$  m from the right road boundary. Each vehicle allocated to zone  $l$  is laterally centered at  $y(0) = y_l + \psi$ , with  $\psi$  uniformly distributed within  $[-0.5, 0.5]$ . Eventually, the vehicles in each zone are longitudinally distributed at random (uniformly) along the 1 km of road length, and this assigns to them also a longitudinal initial coordinate  $x(0)$ . The initial longitudinal and lateral speeds of each vehicle are zero. The desired longitudinal speed  $v_x^d$  assigned to a vehicle is a function of its initial lateral position  $y(0)$ , as follows

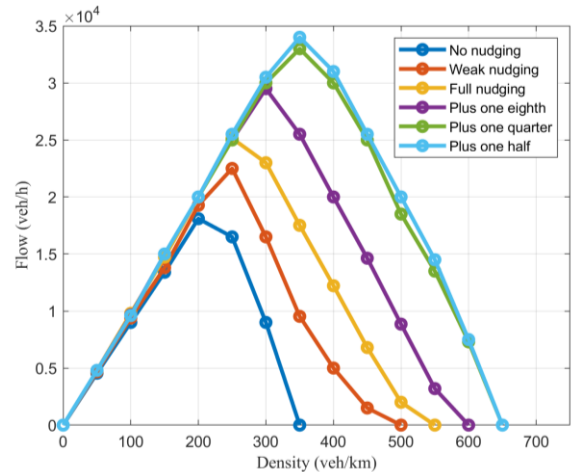


Figure 8. Emerging flow-density curves (Fundamental Diagrams) for various simulated scenarios.

TABLE I. THE DIFFERENT DIMENSION CLASSES OF VEHICLES USED IN THE SIMULATION EXPERIMENT.

	Class 1	Class 2	Class 3	Class 4	Class 5	Class 6
Length (m)	3.20	3.90	4.25	4.55	4.60	5.15
Width (m)	1.60	1.70	1.80	1.82	1.77	1.84

$$v_x^d = 25 + (35 - 25) \frac{y(0)}{10.2} \quad (15)$$

while the desired lateral speed  $v_y^d$  is set equal to 0. Ordering the desired speeds of vehicles according to their initial lateral positioning may increase the resulting traffic flows at lower densities, because faster vehicles are driving farther left and experience therefore less obstructions from encountered slower vehicles; thus, faster vehicles need to apply less decelerations and by-passing maneuvers, which allows them to maintain a higher average speed, as they drive around the ring-road.

The dimensions of each of the  $n$  vehicles placed on the ring-road are determined by choosing randomly (with uniform distribution) one out of the six "dimension classes" reported in Table I.

To obtain each FD, we run a series of simulations employing the vehicle movement strategy settings corresponding to the specific FD scenario. Each simulation in such a series is run for 40 min and produces a point of the corresponding FD, i.e. it produces a density (veh/km) and a flow (veh/h) value. Specifically, each simulation series considers a density  $n = 50, 100, 150, \dots$  veh/km, while traffic flow (in veh/h) is measured at a specific road location and is averaged for the last 5 min of the simulation to produce the stationary traffic flow value corresponding to density  $n$  in the specific FD.

For all produced FDs, the longitudinal time-gap-like parameter is set to  $T_x = 0.20$  s, and the lateral one is set to  $T_y = 0.35$  s. Additionally, we have  $L_{sy} = 0.6$  m,  $D_{sy} = 0.65$  m,  $c_s = 0.3$ ,  $d_s = 1.2$  m and  $v_e = 2$  m/s. The constant bounds are  $[u_x^{b-}, u_x^{b+}] = [-3.5, 2.0]$  m/s<sup>2</sup> for the longitudinal acceleration and  $[u_y^{b-}, u_y^{b+}] = [-1.8, 1.8]$  m/s<sup>2</sup> for the lateral acceleration. Also, we use the parameter values  $\alpha = 0.2$ ,  $\beta = 0.03$ ,  $v_{y\_max} = -v_{y\_min} = 1.5$  m/s,  $k_1 = 4$  s<sup>-2</sup> and  $k_2 = 3.75$  s<sup>-1</sup>. The maximum number of upstream (downstream) vehicles  $n^{ng}$  ( $n^{rp}$ ) (taken into account in determining a nudging (repulsive) force exerted on a vehicle) are set to  $n^{ng} = 3$  and  $n^{rp} = 6$  for all scenarios, while  $\Delta = 250$  m and  $a_s = 0.5$ .

The FDs presented in Fig. 8 demonstrate the following features of the TrafficFluid concept:

- The achieved flows and capacity without nudging are much higher than what is usually observed on a conventional three-lane motorway, something that is attributed mainly to the lane-free traffic character. Of course, these flows are obtained for a ring-road without on-ramps and off-ramps, the presence of which would necessitate lateral vehicle movements that would reduce

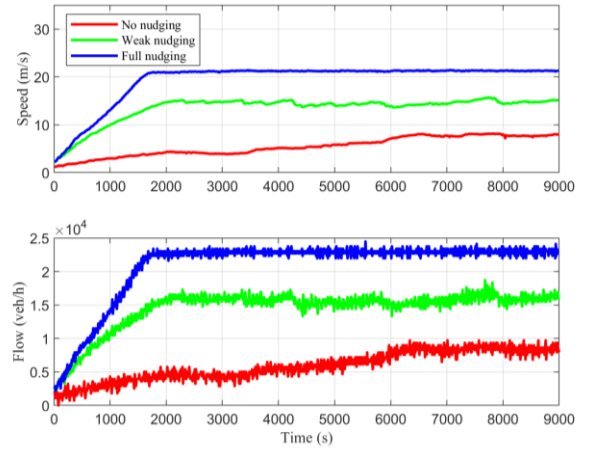


Figure 9. Speed and flow trajectories for three different levels of nudging at an overcritical density (300 veh/km).

the level of achievable flows. Corresponding investigations are ongoing.

- Nudging increases the flows and the capacity, as well as the critical density (at which the highest flow occurs). It was also observed that nudging leads to faster convergence to a quasi-stationary traffic flow and has a stabilizing effect for the traffic flow at higher densities, where less moving waves are observed, something that is compatible with macroscopic observations in [13]; see e.g. Fig. 9, where speed and flow trajectories are presented for three different levels of nudging at the overcritical density of 300 veh/km. The trajectories are seen to converge faster to more stable values as nudging is increased.
- Incremental road widening (by one eighth, one quarter and one half of a "lane") leads to further increases of the flows, the capacity and the maximum density (at which flow and speed return to zero). This is an outstanding characteristic feature of lane-free traffic that is leveraged, with potentially huge benefit, for internal boundary control [16], [17] in the aim of maximizing bi-directional traffic throughput at highways or arterials. Note that in lane-based traffic, flow and capacity increase can only be achieved by widening the road by a whole lane over sufficient highway length. Figure 8 indicates that the increase of flows and capacity is a nonlinear function of the road widening increment. This nonlinear relation is due to different vehicle formations and patterns that emerge and it depends on many factors, including: vehicle sizes and desired speeds, the movement strategy employed, the road width, the road and traffic characteristics (on- and off-ramps) and more.
- Finally, as a common observation for all produced FDs in Fig. 8, the obtained FDs are approximately triangular. More specifically, the left-hand side of all FDs is roughly a straight line with similar slope, which corresponds to the average of the desired vehicle speeds; and the right-hand side of all FDs is roughly linear with similar negative slope, which implies that traffic waves would

move upstream at similar speeds for all investigated scenarios.

Videos of the simulations may be watched at <https://bit.ly/3qumRqL>.

#### IV. CONCLUSION

The TrafficFluid paradigm has been recently proposed for automated vehicles, characterized by two combined principles: lane-free roads and vehicle nudging. This paper presented and employed an ad-hoc vehicle movement strategy for CAVs driving in a lane-free environment, to investigate via simulation some properties of the new traffic paradigm, such as the emerging fundamental diagram, traffic flow capacity, the impact of vehicle nudging and the impact of incremental road widening.

The presented vehicle movement strategy relies on real-time information to decide on longitudinal and lateral accelerations. It was employed for traffic simulation on a ring-road using a recently developed microscopic simulator, called TrafficFluid-Sim. The achieved results demonstrate: safe (crash-free) driving at all densities; high traffic flows and capacity; increase of traffic flows and capacity via vehicle nudging; continuous (albeit nonlinear) capacity increases via incremental road widening. The latter is a property that has been exploited for internal boundary control on highways, in order to flexibly share the total (both directions) road width and capacity among the two directions in dependence of the bi-directional demand and traffic conditions, so as to maximize the total (two directions) flow efficiency [16], [17].

Further extensions and investigations by use of the presented ad-hoc vehicle movement strategy are ongoing for more realistic highway infrastructures, comprising on-ramps and off-ramps, as well as for microscopic testing and demonstration of the internal boundary control concept.

#### REFERENCES

- [1] M. Papageorgiou, C. Diakaki, V. Dinopoulou, A. Kotsialos, and Y. Wang, "Review of road traffic control strategies," *Proceedings of the IEEE*, vol. 91, no. 12, pp. 2043–2067, 2003.
- [2] A. A. Kurzhanskiy, and P. Varaiya, "Active traffic management on road networks: a macroscopic approach," *Philosophical Transactions of the Royal Society A: Mathematical, Physical and Engineering Sciences*, vol. 368, no. 1928, pp. 4607–4626, 2010.
- [3] C. Diakaki, M. Papageorgiou, I. Papamichail, and I. Nikolos, "Overview and analysis of vehicle automation and communication systems from a motorway traffic management perspective," *Transportation Research Part A: Policy and Practice*, vol. 75, pp. 147–165, 2015.
- [4] M. Papageorgiou, K.S. Mountakis, I. Karafyllis, I. Papamichail and Y. Wang. "Lane-free artificial-fluid concept for vehicular traffic," *Proceedings of the IEEE*, vol. 109, no. 2, 2021, pp.114–121.
- [5] V. Kanagaraja, M. Treiber. "Self-driven particle model for mixed traffic and other disordered flows," *Physica A*, vol. 508, pp. 1-11.
- [6] A.K. Mulla, A. Joshi, R. Chavan, D. Chakraborty, D. Manjunath. "A microscopic model for lane-less traffic," *IEEE Transactions on Control of Network Systems*, vol. 6, pp. 415–428, 2019.
- [7] V.K. Yanumula, P. TYPaldos, D. Troullinos, M. Malekzadeh, I. Papamichail and M. Papageorgiou, "Optimal path planning for connected and automated vehicles in lane-free traffic," In *2021 IEEE International Intelligent Transportation Systems Conference (ITSC)*, 2021, pp. 3545–3552.
- [8] I. Karafyllis, D. Theodosis, and M. Papageorgiou. "Two-dimensional cruise control of autonomous vehicles on lane-free roads," In *60th IEEE Conference on Decision and Control (CDC)*, 2021, pp. 2683-2689.
- [9] D. Troullinos, G. Chalkiadakis, I. Papamichail and M. Papageorgiou, "Collaborative multiagent decision making for lane-free autonomous driving". In *Proceedings of the 20th International Conference on Autonomous Agents and MultiAgent Systems*, 2021, pp. 1335–1343.
- [10] M. Papageorgiou, K.S. Mountakis, I. Karafyllis, I. Papamichail. Lane-free artificial-fluid concept for vehicular traffic. 2019, arXiv preprint arXiv:1905.11642.
- [11] D. Troullinos, G. Chalkiadakis, D. Manolis, I. Papamichail and M. Papageorgiou, "Lane-free microscopic simulation for connected and automated vehicles". In *2021 IEEE International Intelligent Transportation Systems Conference (ITSC)*, 2021, pp. 3292–3299.
- [12] P.A. Lopez, M. Behrisch, L. Bieker-Walz, J. Erdmann, Y.-P. Flotterod, R. Hilbrich, L. Lucken, J. Rummel, P. Wagner, and E. Wießner, "Microscopic traffic simulation using sumo," In *21st IEEE International Conference on Intelligent Transportation Systems (ITSC)*, 2018.
- [13] I. Karafyllis, D. Theodosis, M. Papageorgiou. "Analysis and control of a non-local PDE traffic flow model," *International Journal of Control*, vol. 95, pp. 660-678, 2022.
- [14] P. Fancher and Z. Bareket. "Evaluating headway control using range versus range-rate relationships." *Vehicle System Dynamics*, vol. 23, no. 1, 1994, pp.575–596.
- [15] R. Rajamani, *Vehicle dynamics and control*. Springer Science & Business Media, 2011.
- [16] M. Malekzadeh, I. Papamichail, and M. Papageorgiou and K. Bogenberger. "Optimal internal boundary control of lane-free automated vehicle traffic". *Transportation Research Part C: Emerging Technologies*, vol. 126, 2021, Article 103060.
- [17] M. Malekzadeh, I. Papamichail, and M. Papageorgiou, "Linear–Quadratic regulators for internal boundary control of lane-free automated vehicle traffic". *Control Engineering Practice*, vol. 115, 2021, Article 104912.